Drug Design, Development and Therapy

Dovepress
Taylor & Francis Group

Open Access Full Text Article

ORIGINAL RESEARCH

Mechanisms of Microctis Folium in Hyperlipidemia: Integrating Serum Pharmacochemistry, Network Pharmacology, and Transcriptomics

Guanlin Xiao[1], Guangying Wu[2], Yanchang Liu[2], Wanchun Chen[2], Zhihao Zeng[2], Sumei Li[1], Yangxue Li[1], Xiaoli Bi[1]

[1]Guangdong Provincial Engineering Technology Research Institute of Traditional Chinese Medicine/Guangdong Provincial Key Laboratory of Research and Development in Traditional Chinese Medicine, Guangzhou, People's Republic of China; [2]School of the Fifth Clinical Medicine, Guangzhou University of Chinese Medicine, Guangzhou, People's Republic of China

Correspondence: Guanlin Xiao; Xiaoli Bi, Email 164669079@qq.com; zyfxyjs@gzucm.edu.cn

Background: Microctis Folium (MF), a traditional Chinese medicine (TCM), has shown promising effects in treating hyperlipidemia (HLP), yet its active constituents and mechanisms remain largely unclear.

Purpose: This study aimed to systematically elucidate the lipid-lowering effects of MF on high-fat diet (HFD)-induced HLP and identify its pharmacodynamic material basis and molecular mechanism through an integrated multi-omics strategy.

Methods: We developed a UPLC-QTOF-MS/MS method to identify the chemical constituents of MF and the compounds absorbed in rat serum after oral administration of MF. Network pharmacology, molecular docking, and experimental validation were utilized to explore the potential mechanism of MF for the treatment of HLP.

Results: UPLC-QTOF-MS/MS identified 51 chemical compounds in MF and established their material basis. Analysis of serum samples after administration of MF identified 24 enriched compounds as potential active compounds and 597 corresponding prospective targets. Overlaying these compounds with 396 HLP-related genes revealed 101 potential core genes, mainly including AKT1, PTGS2, EGFR, mTOR, and NF-κB. Network pharmacology and transcriptomic analyses indicated that MF regulates key pathways in HLP, notably the PI3K/AKT, mTOR, and NF-κB pathways. Molecular docking further validated the binding affinities of MF key compounds (rutin and isovitexin) to AKT1, mTOR, and NF-κB. In vivo studies confirmed MF's lipid-lowering effects of MF in alleviating HFD-induced lipid accumulation. Compared to the HFD group, MF treatment significantly reduced serum triglycerides (TG), total cholesterol (TC), and low-density lipoprotein cholesterol (LDL-C) levels while increasing high-density lipoprotein cholesterol (HDL-C) levels. Finally, in vivo experiments confirmed the pivotal role of these pathways in the therapeutic effects of MF on HLP.

Conclusion: The comprehensive approach adopted in this study reveals the molecular mechanism of MF for the treatment of HFD-induced HLP, lays an important foundation for elucidating the pharmacological and material basis of the therapeutic effects of MF, and highlights the value of multi-omics integration in TCM research.

Keywords: *Pothos chinensis* (Raf.) Merr, hyperlipidemia, network pharmacology, serum pharmacochemistry, transcriptomics

Introduction

Hyperlipidemia (HLP) is a common metabolic disorder and a major risk factor for cardiovascular disease, stroke, myocardial infarction, and atherosclerosis, posing a significant threat to public health. It is characterized by elevated levels of triglycerides (TG), total cholesterol (TC), and low-density lipoprotein cholesterol (LDL-C), alongside reduced levels of high-density lipoprotein cholesterol (HDL-C).[1] Statins and fibrates are the most widely used lipid-lowering agents; however, their long-term use is often associated with adverse effects such as hepatotoxicity,

Received: 2 April 2025
Accepted: 2 July 2025
Published: 11 July 2025

rhabdomyolysis, and dermatologic reactions.[2,3] As a result, there is an increasing demand for safer, natural, and more effective alternatives. Additionally, recent studies suggest that dyslipidemia and chronic inflammation jointly contribute to the progression of HLP, emphasizing the importance of targeting inflammatory pathways in therapeutic strategies.[4]

Microctis Folium (MF) is the dried leaves of *Microcos paniculata* L., which is included in the 2020 edition of "Pharmacopoeia of the People's Republic of China" and "Catalog of New Resource Foods" of the Ministry of Health of the People's Republic of China.[5–8] As a dual-purpose herb with both medicinal and edible applications, MF has been widely used in traditional Chinese medicine (TCM) and the herbal tea industry. Pharmacological studies and clinical applications have shown that MF exhibits lipid-lowering, anti-inflammatory, antioxidant, analgesic, and gastrointestinal motility-promoting effects.[6,9,10] MF contains diverse bioactive compounds including flavonoids, alkaloids, triterpenoids, steroids, and phenolic acids. Among these, flavonoids and alkaloids have demonstrated lipid-lowering and hepatoprotective activities through mechanisms such as modulating lipid metabolism, inhibiting lipid peroxidation, and reducing inflammatory responses.[7,8] Compared to statins, which act through a single target (HMG-CoA reductase), MF has a broader mechanism of action, controlling high-fat diet-induced HLP while reducing side effects such as hepatotoxicity or rhabdomyolysis. Notably, flavonoids and alkaloids can prevent and treat HLP by inhibiting lipid peroxidation and endogenous lipid biosynthesis while promoting lipid redistribution and exogenous lipid metabolism. Flavonoids and alkaloids can also reduce blood lipid levels by increasing peroxisome proliferator-activated receptor (PPAR-α) expression in the liver, inhibiting 3-hydroxy-3-methylglutaryl coenzyme A reductase and intestinal Acyl-CoA: cholesterol acyltransferase (ACAT) activities, and modulating the activity of lipid-related enzymes. In addition, flavonoids were effective in lowering lipid levels, which may be associated with decreased diacylglycerol acyltransferase (DGAT) and β-Hydroxy -β-methylglutaryl-CoA (HMG-CoA) activities, and increased 7-alpha-hydroxylase and hepatic triglyceride lipase activities.[11,12] To date, the bioactive constituents and mechanism of action of MF in the treatment of HLP have been explored. Modern pharmacological studies have shown that MF can significantly reduce the levels of TC, TG, LDL-C, AST, and ALT, and significantly increase the level of HDL-C in the serum of HLP mice, rats, and NAFLD mice, with lipid-lowering, hepatoprotective, and anti-oxidative stress effects.[8–10,13] Clinical studies have shown that in the treatment of patients with dyslipidemia, the increased use of MF based on TCM lipid-lowering soup can significantly improve the levels of various lipid indicators in patients with dyslipidemia and reduce the risk of atherosclerosis.[14] The above results indicate that MF can regulate lipid metabolism. However, the material basis and mechanism of MF treatment in HLP have not yet been elucidated, which affects the clinical application and further studies of MF.

Owing to the fact that TCM is a complex system of interactions with multiple components, targets, and pathways of action, elucidating the action mechanism of the disease requires a systematic strategy that integrates chemical composition in vivo and in vitro, network pharmacology, transcriptomics, biomarker forecasting, and experimental verification.[15,16] Serum pharmacochemistry is widely used to analyze and screen for active compounds in TCM, ie, compounds appearing by absorption in the blood after oral or intragastric administration of TCM may be significant compounds that are biologically active in vivo.[3,17] Serum pharmacochemistry and network pharmacology have been successfully integrated to elucidate the multi-component synergistic mechanisms of TCM.[18] There is growing evidence that results based on components absorbed into the bloodstream are more accurate and reliable through network pharmacology and transcriptomics analysis.[18,19] Integrating serum pharmacochemistry with network pharmacology and transcriptomics enhances the identification of MF's bioactive components by focusing on compounds absorbed into the bloodstream, which are more likely to exert pharmacological effects in vivo. Compared to traditional in vitro screening, this approach improves biological relevance and allows the prediction and validation of key targets and pathways through multi-omics analysis.

Therefore, in this study, we first characterized the chemical profile of MF both in vitro and in rat serum using UPLC-QTOF-MS/MS. We then combined serum pharmacochemistry, network pharmacology, molecular docking, and transcriptomic analysis to identify the bioactive compounds and elucidate the mechanisms of MF in treating high-fat diet (HFD)-induced HLP. These findings were further validated through in vivo experiments, providing a comprehensive basis for the development of MF as a multi-target therapeutic agent for hyperlipidemia.

Materials and Methods

Reagents

Salicylic acid (0845–9501), 6,7-dihydroxycoumarin (110741–200506), Schaftoside (111912–201703), Ferulic acid (-110773–201313), Vitexin (111687–200602), Isoferulic acid (111698–201103), Rutin (100080–202012), Isorhamnetin-3-O-neohesperidoside (111571–201205), Narcissoside (111571–201205), with purity>98%, were purchased from the national institutes for food and drug control (Beijing, China). Isoschaftoside (Y-153-190626), typhaneoside (X-020-120305), isovitexin (Y-116-120630), Apigenin-7-glucuronide (Q-072-180601), *N*-trans-feruloyltyramine (RFS-F033021080; purity>97%) were purchased from Chengdu Herbpurify Co., Ltd. (Chengdu, China). Isoviolanthin (AF802613), Isoquercitrin (AF7070301), Violanthin (AF802612), 4-Hydroxycinnamic acid (AF20041951), *N*-*p*-trans-coumaroyltyramine (AF22032709), with purity>98%, were provided by Chengdu Abphyto Co., Ltd. (Chengdu, China). Kaempferol-3-β-lucuronide (DSTDS017501), Astragalin (DSTDZ000101), Nicotiflorin (PRF8070724), Tiliroside (PRF9101501), Berberine (PRF7091801), Luteolin-7-*O*-glucuronide (DST221019), with purity>98%, were purchased from Chengdu Purifa Co., Ltd. (Chengdu, China).

Microctis Folium (MF), the dried leaves of *Microcos paniculata* L., a plant native to southern China, was provided by Guangdong Efong Pharmaceutical Co., Ltd. (Guangzhou, China). The plant material was authenticated by experts at the Guangdong Provincial Engineering Technology Research Institute of Traditional Chinese Medicine (TCM).

Preparation of MF Extracts

Coarse MF powder (100 g) was mixed with 2 L 50% ethanol and refluxed for 2 h. The resulting extract was filtered and concentrated to dryness using a rotary evaporator. The dried MF extract was stored at 4 °C until further use.

Animals and Treatments

All animal experiments were approved by the Guangdong Provincial Engineering Technology Research Institute of TCM and were conducted according to the ARRIVE guidelines. During the study, rats and mice were housed in a temperature-controlled environment (24 ± 2 °C) with 60 ± 10% humidity under a standard 12-hour light/dark cycle, with ad libitum access to food and water. Male Sprague-Dawley (SD) rats (200 ± 20 g) were obtained from Guangdong Medical Laboratory Animal Center (Guangzhou, China). Following a one-week acclimation period, all rats underwent a 12-hour fasting period with free access to water before the experiment. 6 rats were administered 5.28 g/kg MF (twice the clinical dosage) via oral gavage, whereas the blank group received water. Blood samples were extracted from the fundus venous plexus 0, 0.083, 0.25, 0.5, 1, 2, 4, 6, 8, 10, 12, and 24 h after administration. Blood samples were immediately centrifuged at 3000 rpm at 4 °C for 15 min to obtain serum, which was then mixed in equal amounts from the above 12 time points and stored at −80 °C until further handling and analysis.[20,21]

Fifty C57BL/6 mice were obtained from Guangdong Medical Laboratory Animal Center (Guangzhou, China). Ten mice were fed a normal chow diet as the normal control (NC group, n=10). The remaining mice were fed a high-fat diet throughout the experiment (HFD model group, n = 40). Blood samples were collected from the orbital vein after four weeks of HFD feeding. Serum levels of TC, TG, HDL-C, and LDL-C were quantified using kits.[22] Forty mice from the high-fat diet model group were randomly divided into four groups according to lipid levels: high-fat diet (HFD) group, HFD+atorvastatin calcium (AT) (10 mg/kg/day), HFD+MF group (MFL) (5.28 g/kg/day) (MFH) 10.56 g/kg/day). All mice were executed after 6 weeks after MF administration, and serum samples were collected by centrifugation at 3000 rpm for 15 min.[21,23] Fresh organs were quickly removed, weighed, and all samples were stored at a temperature of −80 °C before analysis, and a piece of liver was fixed with an amount of 4% paraformaldehyde.

Chemical Profile of MF

MF extract powder was dissolved in 50% methanol, sonicated for 30 min, and centrifuged at 13,000 rpm for 15 min at 4 °C. The supernatant was filtered through a 0.22 μm membrane for UPLC-Q-TOF-MS/MS analysis.

Absorbed Ingredients Identification

To precipitate serum proteins, methanol (4× volume) was added to serum from MF-treated rats. The mixture was vortexed, centrifuged (13,000 rpm, 15 min, 4 °C), evaporated under nitrogen, and reconstituted in 100 μL methanol. After a final centrifugation step, the supernatant was used for UPLC-Q-TOF-MS/MS analysis.[24]

UPLC-Q-TOF-MS/MS Method for Chemical Profile and Serum Pharmacochemistry Analysis

The sample extracts were analyzed using a UPLC-QTOF-MS/MS system (UPLC: 1290II, Agilent; MS: X500R, AB SCIEX). Chromatographic separation was performed at 40°C on a Waters UPLC BEH C18 column (2.1 mm × 100 mm, 1.7 μm) at a flow rate of 0.25 mL/min and an injection volume of 1 μL. The mobile phase involved gradient elution with methanol (A) and 0.1% formic acid in water (B) under the following conditions: 0–4 min, 14–30% A; 4–16 min, 30–58% A; 16–25 min, 58–78% A; 25–30 min, 78–98% A. Both positive and negative modes of electrospray ionization (ESI) were used. The source optimization parameters were set as follows: ion spray voltage: −4.5 kV for negative mode and +5.5 kV for positive mode; atomization gas pressure (Gas 1) and auxiliary gas (Gas 2) pressure: 55 psi; air curtain (Cur) pressure: 35 psi; ion source temperature: 500 °C; mass range: *m*/*z* 50–1000; and collision energy: 30 eV± 15 eV.

Characterization of Prototype Compounds

Total ion chromatograms (TICs) were analyzed using PeakView (v2.0.4) to identify prototypes (absorbed compounds) of MF in rat plasma. The prototypes are present in the plasma samples of the administered group but absent in the control group were identified based on an internal database, secondary fragment ions, and standard compound comparisons.

Network Pharmacology

Potential targets of the identified compounds were predicted using the Traditional Chinese Medicine Systems Pharmacology (TCMSP) and SwissTargetPrediction databases.[21,25] Hyperlipidemia-related disease targets were retrieved from the GeneCards, CTD, and DisGeNet databases using the keyword "hyperlipidemia." Compound-associated and inflammation-related targets were integrated using the Venny 2.1 tool. Protein-protein interaction (PPI) networks were constructed and analyzed using Cytoscape 3.7.1. Functional enrichment analyses, including Gene Ontology (GO) and Kyoto Encyclopedia of Genes and Genomes (KEGG) pathway analyses, were conducted using the DAVID database.[25] GO terms and KEGG pathways with p-values below 0.05 were considered significantly enriched. The top 20 KEGG pathways and top 10 GO terms were preliminarily ranked based on the lowest p-value to prioritize those pathways with the highest statistical evidence of enrichment.[26]

Molecular Docking

Molecular docking simulations were performed using AutoDockTools 1.5.6 and AutoDock Vina v1.1.2 to assess binding affinities between core MF compounds and key target proteins identified through network pharmacology.[20,27]

Biochemical Analysis

The serum levels of TC, TG, LDL-C, and HDL-C were measured using biochemical kits, following the manufacturer's instructions.

Histological Analysis

Liver tissues were fixed in 4% paraformaldehyde for 48 h, followed by dehydration, paraffin embedding, sectioning, and hematoxylin and eosin (H&E) staining. Additionally, the fixed liver samples were rinsed with saline to remove residual paraformaldehyde, treated with 60% isopropyl alcohol, and stained with Oil Red O.

Table 1 Primer Sequences

Gene name	Forward Primer (5′-3′)	Reverse Primer (5′-3′)
IL-6	AGTTGTGCAATGGCAATTCTGA	CTCTGAAGGACTCTGGCTTTGTC
IL-1β	TTGAGTCTGCACAGTTCCCC	GTCCTGGGGAAGGCATTAGG
TNF	CCCTCACACTCACAAACCACC	CTTTGAGATCCATGCCGTTG
AKT	GTCATCGAACGCACCTTCCAT	AGCTTCAGGTACTCAAACTCGT
PI3KCA	AGTAGGCAACCGTGAAGAAAAG	GAGGTGAATTGAGGTCC
mTOR	GCAGATTTGCCAACTATCTTCGG	CAGCGGTAAAAGTGTCCCCTG
GAPDH	GGAGCGAGATCCCTCCAAAAT	GGCTGTTGTCATACTTCTCATGG

Transcriptomics Analysis

Total RNA was isolated from the liver tissues of control, HFD, and MFH+HFD mice using the TRIzol reagent. cDNA libraries were constructed by Shanghai OE Biotech Co. Ltd. (Shanghai, China) and subsequently sequenced using the Illumina Novaseq 6000/MGISEQ-T7 system, according to established protocols. Intergroup differentially expressed genes (DEGs) were identified by the "limma" package in R using $|\log2(\text{Fold Change})| > 0.58$ and p-values below 0.05 as cutoffs. Functional enrichment analyses of DEGs in the HFD versus control and HFD versus MFH groups were performed using Metascape.

Real-Time PCR

Total RNA was extracted from liver tissues using the TRIzol reagent. Reverse transcription was performed using the M-MuLV First Strand cDNA Synthesis Kit, and quantitative real-time PCR (RT-qPCR) was conducted using the 2X SG Fast qPCR Master Mix.[28] RT-qPCR was carried to the manufacturer's protocol, on a StepOnePlus system (USA). Primer sequences used in this study are listed in Table 1. The relative gene expression levels were normalized to those of GAPDH and quantified using the $2^{-\Delta\Delta Ct}$ method.

Statistical Analysis

All data are presented as the mean ± standard deviation. For groups with a sample size of $n \geq 5$, comparisons were conducted using one-way analysis of variance (ANOVA) followed by Tukey's multiple comparison test. For groups with $n < 5$, non-parametric methods including permutation tests were employed to account for the small sample size and lack of normal distribution assumptions. Statistical analyses were performed using GraphPad Prism 9.0. A p-value of less than 0.05 was considered statistically significant.

Results

Identification of Absorbed Components of MF

A total of 51 chemical components of MF and 24 prototypical components of in vivo absorption were characterized using standards, internal databases, and MS/MS fragmentation rules (Figure 1A and B and Table 2. The prototypes identified in both the administered plasma samples and MF, but not in the blank plasma, were absorbed by the MF in rat plasma. The 24 prototype components were confirmed by comparison with the standards (Table 3), and the TICs are shown in Figure 1C–F.

Network Pharmacology Results

Using the Swiss Target Prediction and TCMSP databases, we identified 597 targets related to absorption into blood components. Simultaneously, 396 HLP-related genes were retrieved from the GeneCards, CTD, and DisGeNET databases. By intersecting these datasets using the Venny tool, 101 common targets were identified (Figure 2A), which were considered potential anti-hyperlipidemic targets of MF. These 101 intersecting targets were imported into the STRING database for protein-protein interaction (PPI) analysis, and the resulting network—constructed using Cytoscape 3.7.1—contained 101 nodes and 1948 edges. Based on topological parameters, the top 20 hub genes with the highest degree values were identified

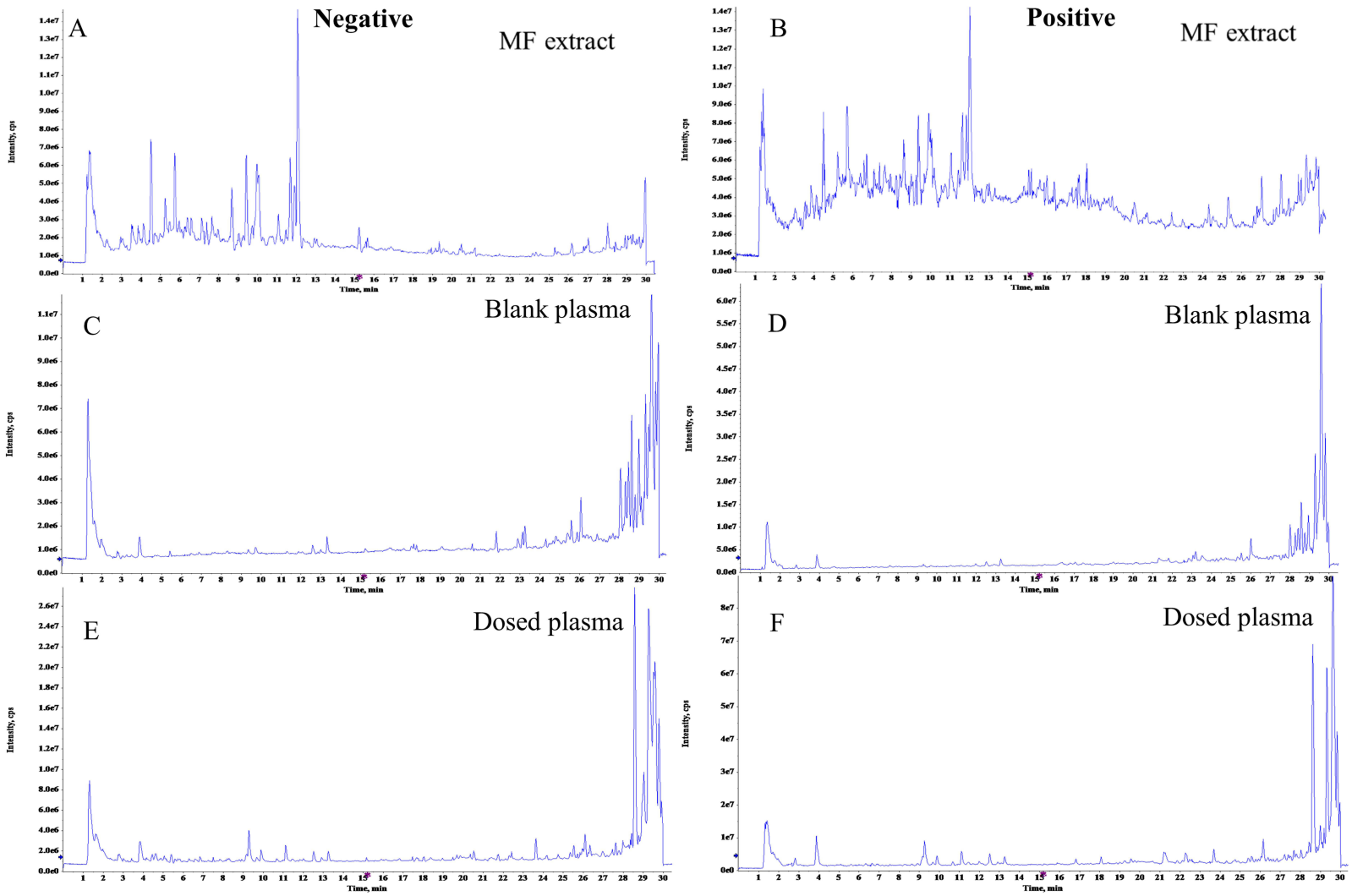

Figure 1 Total ion chromatogram of MF extract, blank plasma, and dosed plasma samples in negative (**A, C** and **E**) and positive (**B, D** and **F**) modes, respectively.

https://doi.org/10.2147/DDDT.S532052

Table 2 Chemical Composition Identification and Analysis Results of MF Extracts

No.	t_R/min	Identification	Formula	Found Mass *m/z*	Error /ppm	MS/MS
1	2.12	Gallic acid	$C_7H_6O_5$	169.014 8 $[M-H]^-$	3.0	125.025 0,79.018 5
2[a]	3.29	Protocatechuic acid	$C_7H_6O_4$	153.019 5 $[M-H]^-$	1.4	109.029 1,108.021 4
3	3.88	B-type proanthocyanidin trimer	$C_{45}H_{38}O_{18}$	865.197 8 $[M-H]^-$ 867.212 6 $[M+H]^+$	−0.9 −0.6	577.137 6,425.089 5,407.078 6,287.056 8 579.150 2,409.092 6,291.087 0
4[a]	4.11	Salicylic acid	$C_7H_6O_3$	137.024 6$[M-H]^-$	1.2	109.030 1,108.021 9,92.027 1,81.035 0
5	4.12	3,4-dihydroxybenzaldehyde	$C_7H_6O_3$	137.024 6 $[M-H]^-$	1.2	108.021 9,92.027 2,81.035 3
6	4.14	Catechin	$C_{15}H_{14}O_6$	289.071 5 [M-H]-	−0.8	203.071 9,247.060 3,123.011 5,109.029 4
7	4.50	B-type proanthocyanidin dimer	$C_{30}H_{26}O_{12}$	577.132 8 $[M-H]^-$	−4.1	559.124 5,425.086 6,407.076 5,289.070 8,205.050 5
				579.148 9$[M+H]^+$	−1.3	427.101 5,409.090 8,291.087 1
8[a]	4.52	Procyanidin B_2	$C_{30}H_{26}O_{12}$	577.133 7 $[M-H]^-$	−2.6	559.126 8,425.0862 5,407.075 6,289.070 1,205.050 3
				579.148 9$[M+H]^+$	−1.3	427.101 1,409.090 6,291.085 8
9[a]	4.73	Mangiferin	$C_{19}H_{18}O_{11}$	421.076 5 $[M-H]^-$	−2.6	403.067 9,331.044 3,301.033 1
				423.091 8 $[M+H]^+$	−1.0	303.050 5
10[a]	5.17	6,7-dihydroxycoumarin	$C_9H_6O_4$	177.019 5 $[M-H]^-$	0.9	133.029 9,89.039 7,77.039 9
11	5.25	B-type proanthocyanidin trimer	$C_{45}H_{38}O_{18}$	865.197 7 $[M-H]^-$	−1.0	577.135 3,425.088 1,407.077 0,289.071 1
				867.212 4 $[M+H]^+$	0.3	579.149 3,409.092 2,291.087 0
12	5.36	B-type proanthocyanidin tetramer	$C_{60}H_{50}O_{24}$	1153.261 3$[M-H]^-$	−0.6	865.203 7,577.138 0,425.089 0,407.080 0,289.072 9 867.214 5,579.151 0,409.094 0,291.087 0
13	5.46	4-hydroxybenzaldehyde	$C_7H_6O_5$	121.030 0 [M-H]-	3.9	93.034 1,92.026 7,91.018 5,65.043 5
14[a]	5.49	Caffeic acid	$C_9H_8O_4$	179.034 9 $[M-H]^-$	−0.4	135.044 4
15[a]	5.75	Epicatechin	$C_{15}H_{14}O_6$	289.071 5 $[M-H]^-$	−1.0	271.062 7,245.081 1,229.051 1,227.071 6,205.050 2,203.070 8,203.070 8,187.039 1,179.034 6,161.024 5,161.060 4,137.024 3,125.023 9
				291.086 1 $[M+H]^+$	−0.6	207.066 0,139.038 7,123.043 9
16[a]	7.25	*p*-coumaric acid	$C_9H_8O_3$	163.033 9 $[M-H]^-$	−1.1	119.049 2
17	7.41	Schaftoside isomer	$C_{26}H_{28}O_{14}$	563.139 6 $[M-H]^-$	−1.9	473.109 1,443.098 8,383.076 3,353.065 8
				565.154 7 $[M+H]^+$	−0.9	547.144 6,529.134 3,511.123 7,445.096 0
18	7.69	Schaftoside isomer	$C_{26}H_{28}O_{14}$	563.141 3 $[M-H]^-$	1.1	473.108 8,443.099 0,383.078 3,353.067 2
				565.155 4 $[M+H]^+$	0.4	547.145 0,529.135 3,511.125 3,445.094 0
19	7.84	Vicenin −2	$C_{26}H_{28}O_{13}$	547.144 5 $[M-H]^-$	−2.2	473.108 6,383.076 9,353.065 8,353.065 8
20[a]	7.93	Schaftoside	$C_{26}H_{28}O_{14}$	563.140 5 $[M-H]^-$	−0.1	473.111 5,443.099 4,383.077 5,353.067 8
				565.155 6 $[M+H]^+$	0.7	547.145 4,529.136 2,511.124 3,445.102 4
21[a]	7.96	Ferulic acid	$C_{10}H_{10}O_4$	193.050 5 $[M-H]^-$	−0.9	178.026 6,149.061 3,134.036 4
				195.065 3 $[M+H]^+$	0.5	177.055 4,145.028 4,117.033 6
22	7.98	B-type proanthocyanidin trimer	$C_{45}H_{38}O_{18}$	865.198 2 $[M-H]^-$	−0.4	577.133 1,425.088 5,407.079 7,289.072 2
				867.212 2 $[M+H]^+$	−1.0	579.148 7,409.092 2,291.087 0
23[a]	8.66	Isoferulic acid	$C_{10}H_{10}O_4$	193.051 2 $[M-H]^-$	3.0	178.027 8,133.029 1,134.037 6,132.020 9
24[a]	8.68	Vitexin	$C_{21}H_{20}O_{10}$	431.097 7 $[M-H]^-$	−1.6	311.054 6
				433.112 1 $[M+H]^+$	−1.9	415.102 0,397.090 6,379.081 0,351.086 5,323.090 8,313.069 6,271.060 7
25[a]	9.06	Isoschaftoside	$C_{26}H_{28}O_{14}$	563.139 9 $[M-H]^-$	−1.3	473.110 5,443.098 5,383.077 5,353.066 0
				565.154 3 $[M+H]^+$	−1.6	547.143 5
26[a]	9.40	Typhaneoside	$C_{34}H_{42}O_{20}$	769.219 2 $[M-H]^-$	−0.6	315.050 9
				771.234 9 $[M+H]^+$	0.8	479.120 2,317.065 9
27[a]	9.43	Isovitexin	$C_{21}H_{20}O_{10}$	431.0973 $[M-H]^-$	−2.5	311.052 6
				433.112 5 $[M+H]^+$	−1.0	415.101 2,397.090 5,379.080 9,323.091 3,313.069 1,271.060 9
28[a]	9.91	Isoviolanthin	$C_{27}H_{30}O_{14}$	577.154 8 $[M-H]^-$	−2.5	503.119 9,487.126 8,473.106 0,457.114 4,413.089 2,383.076 1,353.065 8
				579.170 0 $[M+H]^+$	−1.4	561.159 9,543.148 5,525.138 1,355.081 5
29[a]	9.96	Rutin	$C_{27}H_{30}O_{16}$	609.145 6 $[M-H]^-$	−0.8	301.033 8
				611.161 1 $[M+H]^+$	0.7	465.104 0,303.050 4
30[a]	9.98	Isoquercitrin	$C_{21}H_{20}O_{12}$	463.088 1 $[M-H]^-$	−0.1	300.025 8
				465.103 2 $[M+H]^+$	1.0	303.050 0

(*Continued*)

https://doi.org/10.2147/DDDT.S532052

Table 2 (Continued).

No.	t_R/min	Identification	Formula	Found Mass *m/z*	Error /ppm	MS/MS
31[a]	10.07	Violanthin	$C_{27}H_{30}O_{14}$	577.155 5 $[M-H]^-$	−1.4	503.120 7,487.124 1,473.108 9,457.113 0,413.087 8,383.075 7,353.065 2
				579.170 3 $[M+H]^+$	−0.8	561.158 9,543.149 2,525.138 9,355.081 9
32[a]	10.24	Procyanidin A_2	$C_{30}H_{24}O_{12}$	575.119 9 $[M-H]^-$	0.7	423.072 1
				577.134 3 $[M+H]^+$	0.4	425.087 1
33[a]	10.28	Berberine	$C_{20}H_{17}NO_4$	336.123 4 $[M+H]^+$	1.1	320.092 5,304.097 2,278.081 9
34	10.68	Hesperidin	$C_{28}H_{34}O_{15}$	609.182 3 [M-H]-	−0.4	325.072 3,301.070 9,286.048 3,242.058 2
35	11.25	Diosmin	$C_{28}H_{32}O_{15}$	607.167 8 [M-H]-	1.5	449.233 2,341.067 0,299.057 0,284.033 5
36[a]	11.38	*N-p*-trans-coumaroyltyramine	$C_{17}H_{17}NO_3$	282.114 6 $[M-H]^-$	3.6	282.117 4,174.056 3,132.057 4,119.050 5
				284.128 4$[M+H]^+$	0.8	147.044 2,121.065 2
37[a]	11.41	Kaempferol-3-beta-*O*-glucuronide	$C_{21}H_{18}O_{12}$	461.073 8 $[M-H]^-$	2.6	285.041 9,257.045 8,229.051 1
38[a]	11.63	Astragalin	$C_{21}H_{20}O_{11}$	447.093 4 $[M-H]^-$	0.2	285.040 1
				449.108 0 $[M+H]^+$	0.3	287.054 6
39[a]	11.69	Nicotiflorin	$C_{27}H_{30}O_{15}$	593.149 9 $[M-H]^-$	−2.2	285.038 5
				595.165 2 $[M+H]^+$	–0.9	449.107 4,287.053 4
40	11.85	Azelaic acid	$C_{10}H_{18}O_4$	187.097 8$[M-H]^-$	0.9	125.096 6,124.677 2,97.065 6,95.050 4
41[a]	11.87	Isorhamnetin 3-*O*-neohesperidoside	$C_{28}H_{32}O_{16}$	623.161 0 $[M-H]^-$	−1.3	315.050 6
				625.176 0 $[M+H]^+$	−0.5	479.118 2,317.066 0
42	11.93	Quercetin-3-*O*-glucuronide	$C_{21}H_{18}O_{13}$	477.102 2 $[M-H]^-$	72.9	477.101 4,314.041 0,285.039 2,271.023 5,243.028 6
43[a]	11.98	*N*-trans-feruloyltyramine	$C_{18}H_{19}NO_4$	312.124 5 [M-H]-	1.3	296.094 1,190.051 2,178.0516,148.053 5,133.028 0
				314.139 0 $[M+H]^+$	0.9	177.055 0,245.029 3,117.034 1
44[a]	12.07	Narcissoside	$C_{28}H_{32}O_{16}$	623.159 5 $[M-H]^-$	−3.6	315.048 7,300.026 0
				625.176 0 $[M+H]^+$	−0.5	479.117 3,317.064 1,302.042 4
45	13.94	Quercetin	$C_{15}H_{10}O_7$	301.035 4 $[M-H]^-$	0.2	178.999 6,151.003 8,121.045 4,107.014 6,83.014 0
46	14.27	Naringenin	$C_{15}H_{12}O_5$	271.062 0 $[M-H]^-$	2.9	187.041 5,151.004 3,119.050 2,107.013 6,65.003 1
47	15.04	Decanedioic acid	$C_{10}H_{18}O_4$	201.113 9 $[M-H]^-$	3.3	183.102 4,139.113 4,137.096 5,83.049 5
48[a]	15.23	Tiliroside	$C_{30}H_{26}O_{13}$	593.129 7 $[M-H]^-$	−0.6	447.094 8
				595.144 8 $[M+H]^+$	0.4	287.054 8
49	16.27	Luteolin	$C_{15}H_{10}O_6$	285.040 3 $[M-H]^-$	−0.7	229.050 6,185.061 0,151.004 0,93.034 8
50	16.88	Isorhamnetin	$C_{16}H_{12}O_7$	315.050 9 $[M-H]^-$	−0.5	300.027 4,151.003 6
51	17.01	Kaempferol	$C_{16}H_{12}O_6$	299.057 0 $[M-H]^-$	3.0	284.033 2,256.038 9,61.987 6

Note: [a]Identified by comparing with the standards.

Table 3 Identification of Chemical Components in Plasma After Oral Administration of MF Extract

No.	Identification	Formula	Found Mass *m/z*	Error /ppm	MS/MS
S1	Salicylic acid	$C_7H_6O_3$	137.024 6$[M-H]^-$	1.2	109.030 1,108.021 9,92.027 1,81.035 0
S2	6,7-dihydroxycoumarin	$C_9H_6O_4$	177.019 5 $[M-H]^-$	0.9	133.029 9,89.039 7,77.039 9
S3	*p*-coumaric acid	$C_9H_8O_3$	163.033 9 $[M-H]^-$	−1.1	119.049 2
S4	Schaftoside	$C_{26}H_{28}O_{14}$	563.140 5 $[M-H]^-$	−0.1	473.111 5,443.099 4,383.077 5,353.067 8
			565.155 6 $[M+H]^+$	0.7	547.145 4,529.136 2,511.124 3,445.102 4
S5	Ferulic acid	$C_{10}H_{10}O_4$	193.050 5 $[M-H]^-$	−0.9	178.026 6,149.061 3,134.036 4
			195.065 3 $[M+H]^+$	0.5	177.055 4,145.028 4,117.033 6
M1	Apigenin-7-glucuronide	$C_{21}H_{18}O_{11}$	445.078 8 $[M-H]^-$	2.7	269.048 2,146.966 1
S6	Isoferulic acid	$C_{10}H_{10}O_4$	193.051 2 $[M-H]^-$	3.0	178.027 8,133.029 1,134.037 6,132.020 9
S7	Vitexin	$C_{21}H_{20}O_{10}$	431.097 7 $[M-H]^-$	−1.6	311.054 6
			433.112 1 $[M+H]^+$	−1.9	415.102 0,397.090 6,379.081 0,351.086 5,323.090 8,313.069 6,271.060 7
S8	Isoschaftoside	$C_{26}H_{28}O_{14}$	563.139 9 $[M-H]^-$	−1.3	473.110 5,443.098 5,383.077 5,353.066 0
			565.154 3 $[M+H]^+$	−1.6	547.143 5

(*Continued*)

Table 3 (Continued).

No.	Identification	Formula	Found Mass *m/z*	Error /ppm	MS/MS
S9	Typhaneoside	$C_{34}H_{42}O_{20}$	769.219 2 $[M-H]^-$	−0.6	315.050 9
			771.234 9 $[M+H]^+$	0.8	479.120 2,317.065 9
S10	Isovitexin	$C_{21}H_{20}O_{10}$	431.0973 $[M-H]^-$	−2.5	311.052 6
			433.112 5 $[M+H]^+$	−1.0	415.101 2,397.090 5,379.080 9,323.091 3,313.069 1,271.060 9
S11	Isoviolanthin	$C_{27}H_{30}O_{14}$	577.154 8 $[M-H]^-$	−2.5	503.119 9,487.126 8,473.106 0,457.114 4,413.089 2,383.076 1,353.065 8
			579.170 0 $[M+H]^+$	−1.4	561.159 9,543.148 5,525.138 1,355.081 5
S12	Rutin	$C_{27}H_{30}O_{16}$	609.145 6 $[M-H]^-$	−0.8	301.033 8
			611.161 1 $[M+H]^+$	0.7	465.104 0,303.050 4
S13	Isoquercitrin	$C_{21}H_{20}O_{12}$	463.088 1 $[M-H]^-$	−0.1	300.025 8
			465.103 2 $[M+H]^+$	1.0	303.050 0
M2	Luteolin-7-*O*-glucuronide	$C_{21}H_{18}O_{12}$	461.074 4 $[M-H]^-$	3.9	285.041 3,166.910 7
S14	Violanthin	$C_{27}H_{30}O_{14}$	577.155 5 $[M-H]^-$	−1.4	503.120 7,487.124 1,473.108 9,457.113 0,413.087 8,383.075 7,353.065 2
			579.170 3 $[M+H]^+$	−0.8	561.158 9,543.149 2,525.138 9,355.081 9
S15	*N-p*-trans-coumaroyltyramine	$C_{17}H_{17}NO_3$	282.114 6 $[M-H]^-$	3.6	282.117 4,174.056 3,132.057 4,119.050 5
			284.128 4$[M+H]^+$	0.8	147.044 2,121.065 2
S16	Kaempferol-3-beta-*O*-glucuronide	$C_{21}H_{18}O_{12}$	461.073 8 $[M-H]^-$	2.6	285.041 9,257.045 8,229.051 1
S17	Astragalin	$C_{21}H_{20}O_{11}$	447.093 4 $[M-H]^-$	0.2	285.040 1
			449.108 0 $[M+H]^+$	0.3	287.054 6
S18	Nicotiflorin	$C_{27}H_{30}O_{15}$	593.149 9 $[M-H]^-$	−2.2	285.038 5
			595.165 2 $[M+H]^+$	−0.9	449.107 4,287.053 4
S19	*N*-trans-feruloyltyramine	$C_{18}H_{19}NO_4$	312.124 5 [M-H]-	1.3	296.094 1,190.051 2,178.0516,148.053 5,133.028 0
			314.139 0 $[M+H]^+$	0.9	177.055 0,245.029 3,117.034 1
S20	Isorhamnetin 3-*O*-neohesperidoside	$C_{28}H_{32}O_{16}$	623.161 0 $[M-H]^-$	−1.3	315.050 6
			625.176 0 $[M+H]^+$	−0.5	479.118 2,317.066 0
S21	Narcissoside	$C_{28}H_{32}O_{16}$	623.159 5 $[M-H]^-$	−3.6	315.048 7,300.026 0
			625.176 0 $[M+H]^+$	−0.5	479.117 3,317.064 1,302.042 4
S22	Tiliroside	$C_{30}H_{26}O_{13}$	593.129 7 $[M-H]^-$	−0.6	447.094 8
			595.144 8 $[M+H]^+$	0.4	287.054 8

Note: All determined by comparison with standards.

as core targets, including IL6, INS, PTGS2, IL1B, PPARG, AKT1, TNF, TP53, HIF1A, EGFR, NFKB1, MTOR, and CASP3 (Figure 2B). Furthermore, the drug-component-target interaction network revealed that rutin and isovitexin had the highest number of target interactions, with degree values of 12 and 10, respectively (Figure 2C).

GO and KEGG Enrichment Analysis

The top 10 entries in biological processes, molecular functions, and cellular components are displayed from 101 potential targets (Figure 2D). The biological processes include negative regulation of the apoptotic process, response to lipopolysaccharide, and positive regulation of the nitric oxide biosynthetic process. Cellular components include mitochondria, cytoplasm, and transcription factor complexes. Molecular functions include enzyme binding, protein serine/threonine/tyrosine kinase activity, and oxidoreductase activity. Moreover, KEGG pathway analysis indicated that these targets were significantly enriched in pathways such as HIF-1 signaling, PI3K-Akt signaling, insulin resistance, non-alcoholic fatty liver disease, TNF signaling, AMPK signaling, NF-κB signaling, mTOR signaling, PPAR signaling, linoleic acid metabolism, arachidonic acid metabolism, NF-κB signaling, and tryptophan metabolism, which may be the core anti-hyperlipidemia pathways. The top 20 pathways are shown in Figure 2E. As shown in Figure 3, the red-colored protein in the PI3K/AKT/mTOR and NF-κB signaling pathway diagrams represent the enriched targets.

https://doi.org/10.2147/DDDT.S532052

https://doi.org/10.2147/DDDT.S532052

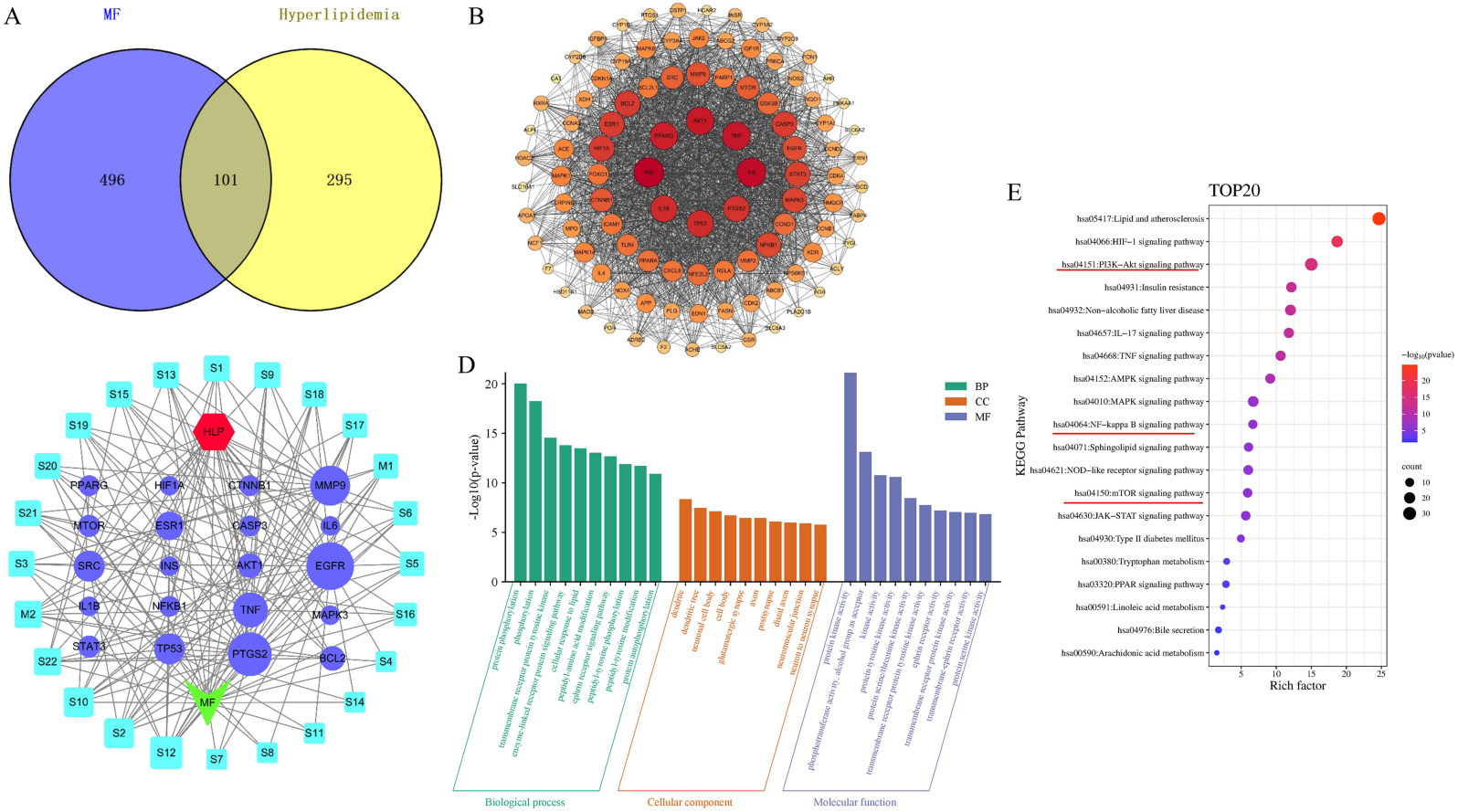

Figure 2 Network pharmacology reveals the mechanism of MF anti-HLP. (**A**) Venny analysis for intersection targets. (**B**) PPI network of MF anti-HLP. (**C**) Drug-component-target network. (**D**) Molecular function analysis, biological process analysis, and cellular component analysis. (**E**) KEGG pathway enrichment.

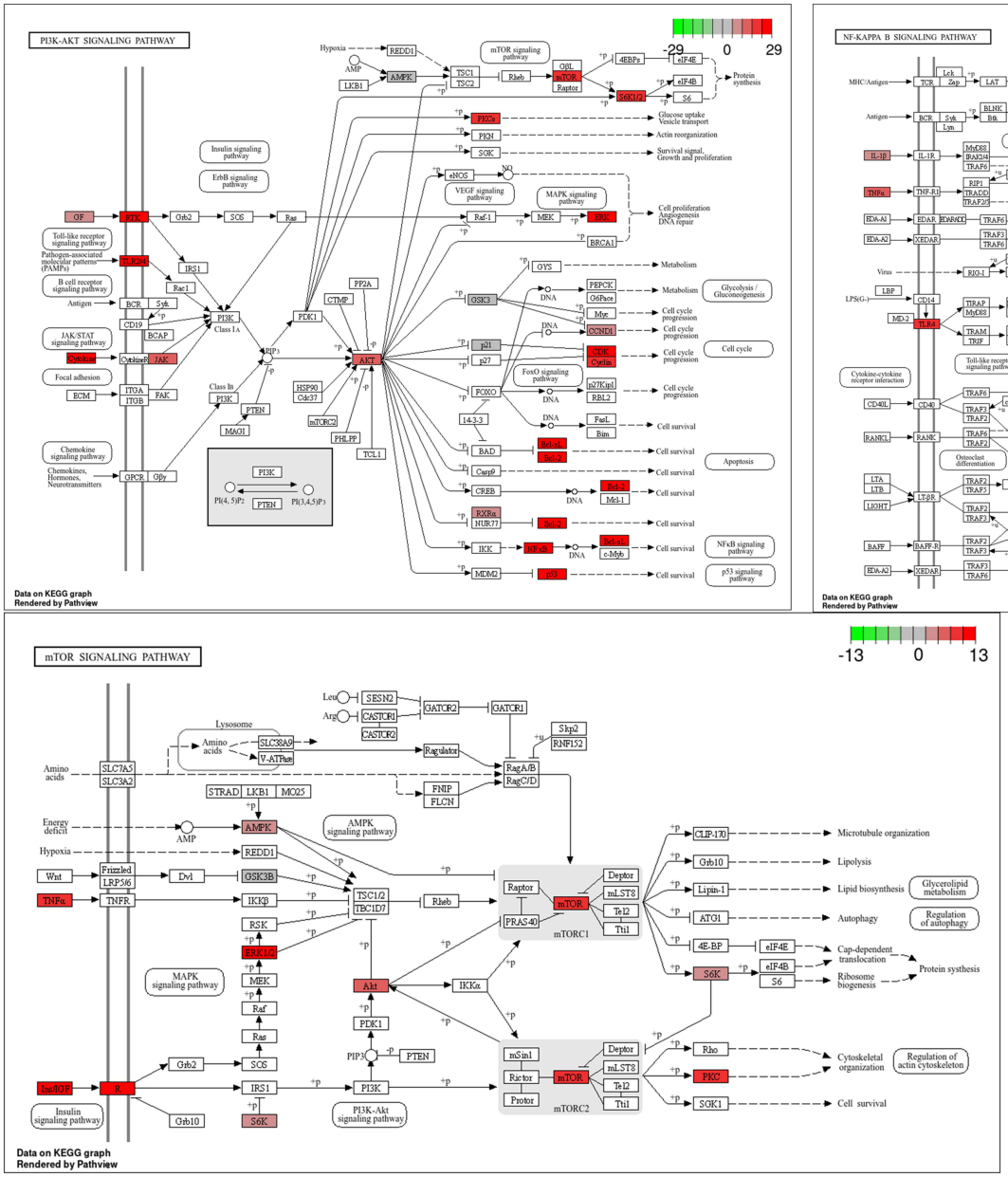

Figure 3 Potential targets of MF on HLP are enriched in PI3K/AKT signaling pathway, NF-KB signaling pathway, and mTOR signaling pathway.

Table 4 Molecular Docking Parameter Table

Compound	Docking Parameters	AKT1	mTOR	NF-κB
Rutin	Binding energy/kJ·mol $^{-1}$	−9.4	−6.2	−7.5
	Participating amino acid residues (H-Bonds/π-Interactions)	H-donor GLN 79, LYS 268/pi-pi TRP 80	H-donor LYS 170, ILE 172, GLN 203, ALA 206/pi-pi PHE 145	H-donor GLN 29, ARG 30, ASN 190, LYS 218, GLN 220
Isovitexin	Binding energy/kJ·mol $^{-1}$	−9.8	−5.2	−7.4
	Participating amino acid residues (H-Bonds/π-Interactions)	H-donor ASN 54, THR 80, TYR 263/pi-pi TRP 80	H-donor TYR 198/pi-pi PHE 145	H-donor GLN 29, LYS 218, GLN 220, GLN 247

Molecular Docking Results

AKT1, mTOR, and NF-κB may be the key targets of MF in the treatment of HLP. Therefore, a molecular docking analysis was conducted to calculate the binding energies of the absorbed components and their targets. The results indicated that the two core compounds, rutin and isovitexin, could bind to multiple binding sites on AKT1, mTOR, and NF-κB proteins with docking scores below −5.0 kcal/mol. The results of molecular docking are presented in Table 4 and Figure 4. The major interaction forms in the figure were π–π and hydrogen bonding, and the docking energies of all conformations were below −5 kcal mol^{-1}, with a standard value of −5.0 kcal mol^{-1} for the binding energy in general. This indicates that the core compounds bind well to the receptor proteins, suggesting that rutin and isoflavone glycosides may have a well-regulated effect on these target proteins.

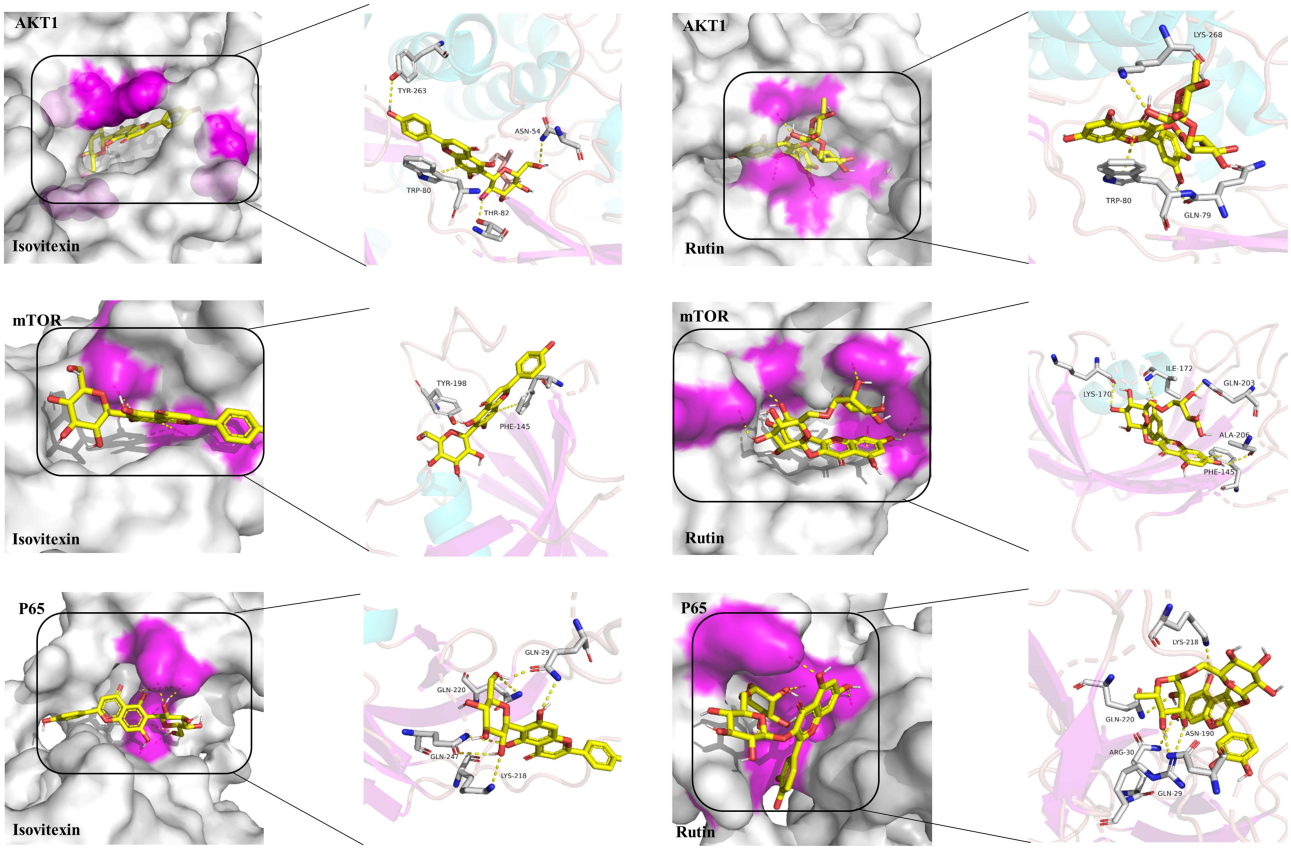

Figure 4 Docking patterns of core targets (AKT1, mTOR, and P65) and core active compounds (Isovitexin, and Rutin) of MF.

Effects of MF on Serum Lipid Profiles

Biochemical assays revealed that MF significantly improved lipid profiles in HFD-induced hyperlipidemic mice. As shown in Figure 5, mice in the HFD group exhibited elevated serum TC, TG, and LDL-C levels and reduced HDL-C levels. In contrast, MF treatment markedly lowered TC, TG, and LDL-C levels while increasing HDL-C, indicating a robust lipid-lowering effect.

H&E and Oil Red O Staining

We further investigated the effect of MF on the liver of HFD-induced hyperlipidemic mice. H&E staining showed that the hepatic lobular structure of the HFD model group was destroyed, with an obvious infiltration of inflammatory cells (Figure 6A). Oil Red O staining showed that the liver tissue was red-stained, and a large number of obvious lipid droplet aggregates were observed in the HFD model group (Figure 6B). Notably, the MF intervention significantly ameliorated these abnormalities.

RNA-Seq Analysis

According to the transcriptomic results, genes with p values < 0.05, fold-change (FC) > 1.5, or FC < 0.67 between the HFD and CON groups, and between the MFH and HFD groups were chosen as differential genes. There were 885 genes

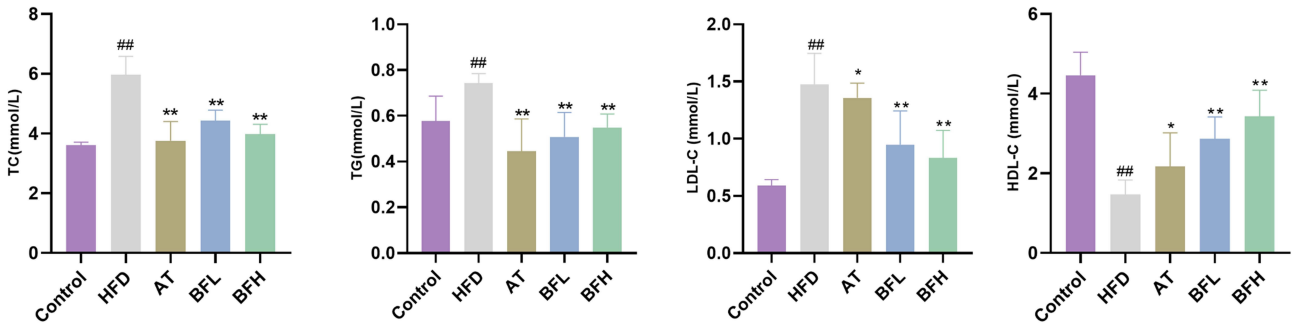

Figure 5 Effects of HFD and MF treatment on serum lipid levels. *p<0.05, **p<0.01 vs the control group, ##p<0.01 vs the HFD group.

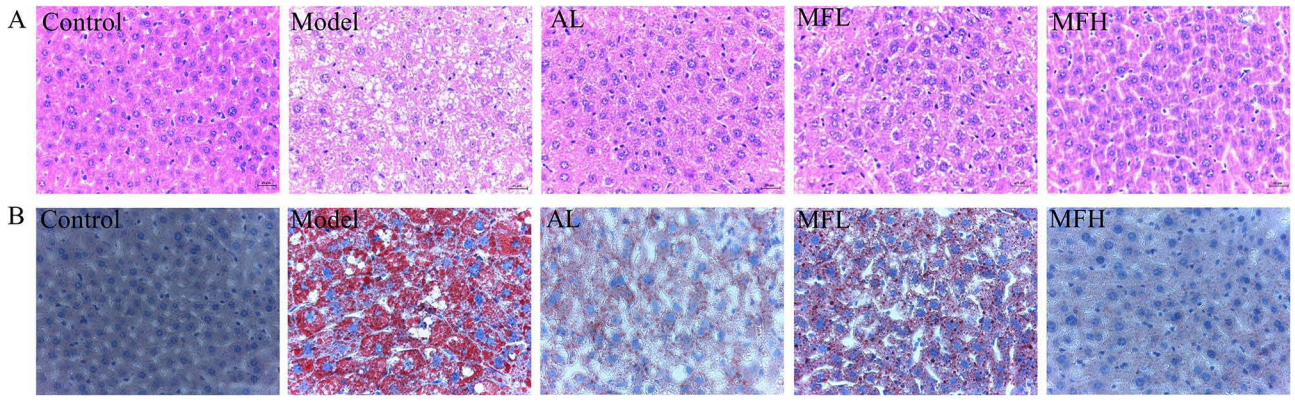

Figure 6 H&E and Oil red O staining. (**A**) Histopathologic sections of liver, H&E stain. (**B**) Oil red O staining section of liver.

https://doi.org/10.2147/DDDT.S532052

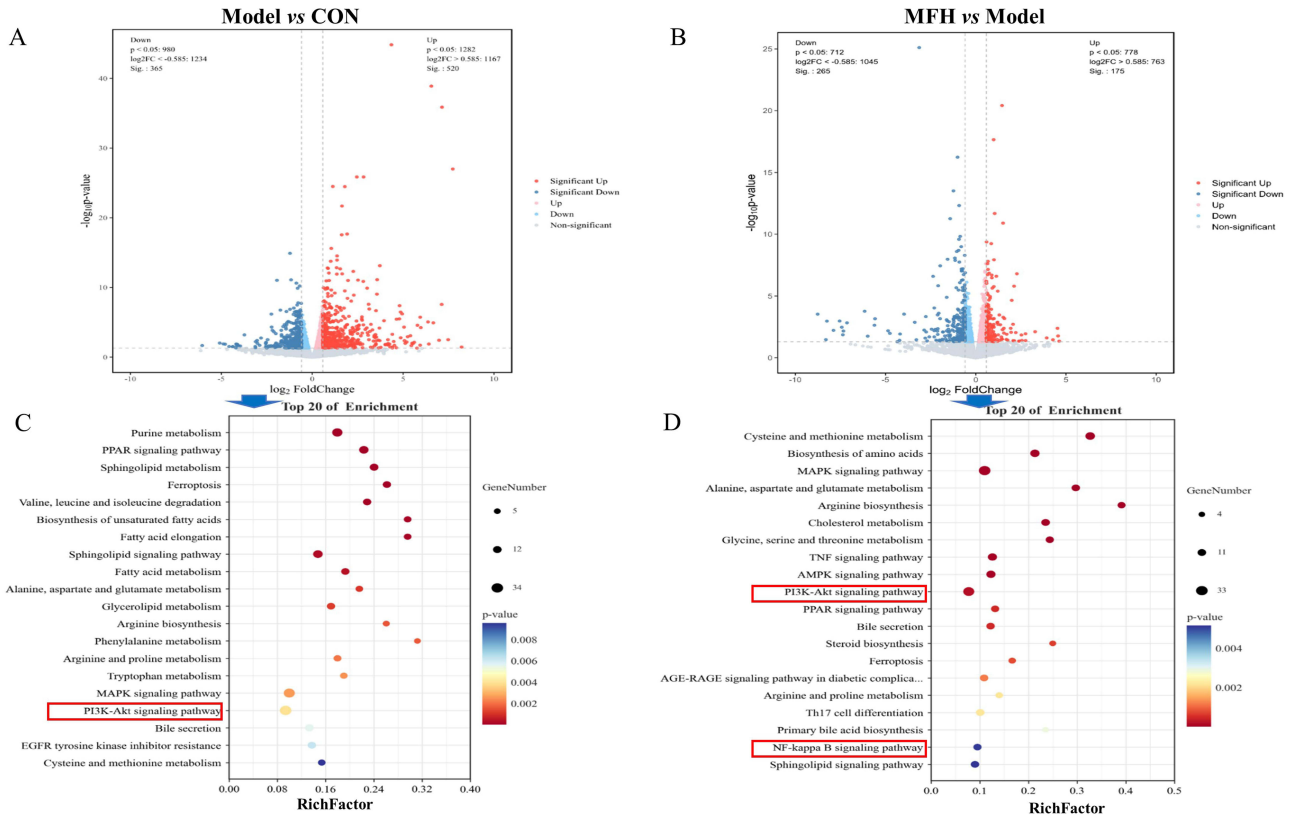

Figure 7 Profiling of DEGs in liver tissues from different groups. (**A** and **B**) Volcano plot showed the differentially regulated genes between HFD and CON, and between MFH and HFD groups. (**C** and **D**) The DEGs from HFD vs CON, MFH vs HFD respectively were enriched in the KEGG pathway database.

exhibiting significant differences between the HFD and NC groups, and 440 genes between the MFH and HFD groups (Figure 7A and B). Differential genes were also enriched and analyzed separately, and the results are presented in Figure 7C and D. Additionally, KEGG pathway analysis of DEGs in the HFD vs CON and MFH vs HFD groups revealed enrichment in the PI3K/Akt and NF-κB signaling pathways (Figure 7C and D). A literature review confirmed the crucial role of these two signaling pathways in the occurrence and progression of HLP.[29,30] Combined with network pharmacology findings, the PI3K/AKT and NF-κB pathways were identified as the key regulatory mechanisms underlying effects of MF on metabolic disorders in HLP mice.

Effects of MF on PI3K/Akt/mTOR and NF-κB Signaling Pathway

Combined with the core targets and pathways predicted by absorption into the blood component network pharmacology, PI3K, Akt, mTOR, and NF-κB may be the key targets of MF-active compounds, and the ameliorating effect of MF on hyperlipidemia may be related to the PI3K/Akt/mTOR and NF-κB signaling pathways. To validate the predicted regulatory mechanisms, RT-qPCR was used to quantify the mRNA expression of key pathway components. Compared with the control group, the HFD group showed significant upregulation of PIK3CA, AKT1, mTOR, TNF-α, IL-1β, and IL-6. MF treatment significantly reversed these increases (Figure 8A), confirming its inhibitory effect on the PI3K/AKT/mTOR and NF-κB signaling pathways. The proposed underlying mechanism of MF in HLP mice is shown in Figure 8B.

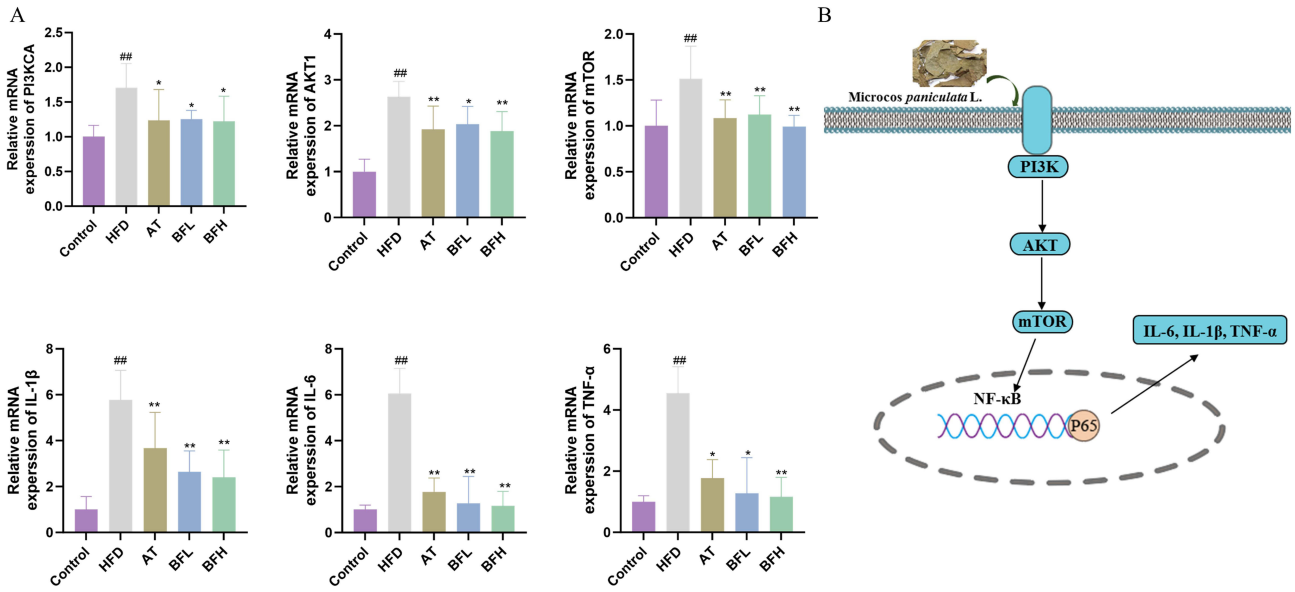

Figure 8 The proposed underlying mechanism of MF in HLP mice. (**A**) The mRNA levels of Akt, mTOR, PIK3CA, TNF-α, IL-1β, and IL-6 in mice liver. Data were presented as the mean ± SD. *$p<0.05$, **$p<0.01$ vs the control group, $^{\#\#}p<0.01$ vs the HFD group. (**B**) Mechanism diagram of MF treatment of HLP.

Discussion

In this study, we comprehensively investigated the active components and underlying mechanisms of MF in the treatment of HLP through an integrated approach combining serum pharmacochemistry, network pharmacology, molecular docking, transcriptomic analysis, and in vivo experimental validation. A total of 24 prototype compounds were identified in the serum of healthy SD rats after oral administration of MF, and their potential targets were predicted using network pharmacology. Subsequent network analysis revealed that AKT1, mTOR, and NF-κB were among the core targets, with rutin and isovitexin emerging as key bioactive compounds. These components are likely to exert their lipid-lowering and anti-inflammatory effects through modulation of the PI3K/AKT/mTOR and NF-κB signaling pathways. Notably, transcriptomic analysis supported the network-based predictions, and RT-qPCR results further confirmed that MF significantly downregulated the mRNA expression of PI3KCA, AKT1, mTOR, TNF, IL-6, and IL-1β. These findings validate the utility of an integrated multi-omics approach for elucidating the pharmacodynamic material basis and molecular mechanisms of MF against HLP.

Identifying the pharmacologically relevant constituents of TCM is essential for clarifying their therapeutic potential. While TCMs contain numerous chemical constituents, not all exert biological effects in vivo. Conventional screening via the TCMSP database often uses criteria such as oral bioavailability (OB ≥ 30%) and drug-likeness (DL ≥ 0.18), but this approach may overlook metabolites or low-OB compounds that demonstrate significant bioactivity after metabolism.[17] In contrast, serum pharmacochemistry focuses on components that are actually absorbed into the bloodstream following administration, providing a more accurate reflection of bioactive substances. In this study, 51 compounds (including flavonoids, organic acids, proanthocyanidins, and amides) were characterized from MF based on high-resolution MS data, literature comparison, and reference standards. Among them, 24 prototype compounds were detected in rat plasma and identified as candidate bioactive components. The remaining compounds may have been undetectable due to low abundance or metabolic transformation into Phase I or II metabolites. These 24 absorbed compounds, particularly flavonoids, alkaloids, and organic acids, are known for their regulatory effects on lipid metabolism and inflammation. For example, isovitexin has been shown to inhibit NF-κB translocation and MAPK phosphorylation, thereby exerting potent anti-inflammatory effects.[31] Rutin and vitexin have demonstrated lipid-lowering properties by improving hepatic lipid accumulation, reducing inflammation, and restoring glucose-lipid metabolism in HLP and NAFLD models.[32–35] Similarly, phenolic acids such as ferulic and caffeic acids have been reported to modulate oxidative stress and lipid-related pathways.[36] The synergistic action of these blood-absorbed compounds likely underpins MF's dual lipid-

https://doi.org/10.2147/DDDT.S532052

regulatory and anti-inflammatory effects. Therefore, these components may serve as the core pharmacologically active substances responsible for the therapeutic efficacy of MF in HLP management.

The analysis showed that the 101 overlapping targets of compound-related targets and HLP-related genes mainly involved the PI3K/AKT/mTOR and NF-κB signaling pathways, which proved that these two pathways were highly related to HLP. These results were consistent with in vivo experimental validation, which demonstrated the therapeutic effects of MF in a high-fat diet (HFD)-induced HLP mouse model. Specifically, MF administration significantly reduced serum levels of TG, TC, and LDL-C, while increasing HDL-C, and alleviated hepatic lipid accumulation. Excessive hepatic lipid deposition is a hallmark of HLP and can lead to liver injury and inflammatory responses.[37] RT-qPCR analysis further confirmed that MF significantly suppressed the expression of PI3K, AKT, mTOR, TNF-α, IL-6, and IL-1β mRNA in liver tissues, supporting the hypothesis that MF exerts its lipid-lowering and anti-inflammatory effects through inhibition of both PI3K/AKT/mTOR and NF-κB pathways. Previous studies have confirmed that these two pathways are strongly associated with HLP.[4]

The liver plays a central role in lipid metabolism and inflammation.[4] The NF-κB signaling pathway is a major regulator of inflammatory responses, particularly through the transcriptional activation of pro-inflammatory cytokines such as IL-6 and TNF-α. Hyperactivation of this pathway contributes to hepatic inflammation and injury in HLP and NAFLD. In addition, Akt can activate NF-κB signaling by phosphorylating IKKα, and activation of IKKα/β kinase promotes the release of NF-κB dimers, which translocate to the nucleus to associate with target genes and promote the transcription of pro-inflammatory factors (eg, IL-6 and IL-1β).[4,35] Meanwhile, the PI3K/Akt/mTOR pathway is involved in many intracellular activities in cell growth, proliferation, apoptosis, and autophagy, and plays an important role in a variety of diseases such as HLP, atherosclerosis, NAFLD, and inflammatory bowel disease.[38–40] Inhibition of the PI3K/AKT signaling pathway reduces hepatocyte injury and lipid disorders in HFD-induced HLP and NAFLD animal models.[41,42] mTOR is one of the key downstream targets of the PI3K/AKT pathway, which together with the upstream is known as the PI3K/AKT/mTOR pathway. mTOR forms two distinct complexes, mTORC1 and mTORC2. mTORC1 and mTORC2 have different roles in the PI3K/AKT/ mTOR signaling pathway, but both are closely related to the pathogenesis of obesity.[43]

In summary, our findings suggest that MF exerts multi-targeted therapeutic effects in HLP by simultaneously modulating the PI3K/AKT/mTOR and NF-κB signaling pathways, thereby reducing lipid accumulation and inflammation. Key absorbed compounds such as rutin and isovitexin were shown to interact with core targets (AKT1, mTOR, NF-κB), providing a pharmacological basis for the efficacy of MF. These results were corroborated by transcriptomic profiling and RT-qPCR validation. Compared to conventional therapies like statins that primarily act on cholesterol synthesis, MF offers a broader and potentially safer strategy for managing HLP, especially in patients with concurrent inflammatory complications. Nonetheless, several limitations should be acknowledged. The sample size for RNA sequencing was relatively small (n=3 per group), which, while common in exploratory omics studies, may reduce statistical power and increase variability.[44,45] Additionally, pooled serum samples were used for pharmacokinetic screening, which limits insight into inter-individual variability. Future studies should increase the number of biological replicates, employ proteomics for deeper mechanistic validation, and apply pharmacokinetic modeling to optimize dosing strategies. Moreover, despite the observed in vivo efficacy via oral gavage, many of MF's flavonoids exhibit poor solubility and bioavailability. This highlights the need for advanced formulation strategies, such as nanoparticle delivery systems or non-aqueous parenteral formulations, to enhance clinical translation. These efforts will be critical in developing MF into a standardized, effective, and widely accepted therapeutic agent for the treatment of HLP.

Conclusions

In this study, we integrated serum pharmacochemistry, network pharmacology, and transcriptomic analyses to identify the bioactive components and elucidate the molecular mechanisms of MF in the treatment of HLP. Our findings demonstrate that MF alleviates lipid accumulation and inflammation primarily through modulation of the PI3K/AKT/mTOR and NF-κB signaling pathways. This work provides a scientific basis for understanding the pharmacological efficacy of MF and offers theoretical support for its clinical application in managing HLP. Moreover, the study presents a novel and systematic approach for exploring the active constituents and mechanisms of TCM, contributing valuable insights to the modernization and mechanistic investigation of herbal therapies.

Abbreviations

ACAT, Acyl-CoA:cholesterol acyltransferase; AT, atorvastatin calcium; DGAT, diacylglycerol acyltransferase; GO, Gene Ontology; HMG-CoA, β-Hydroxy β-methylglutaryl-CoA; HDL-C, high-density lipoprotein cholesterol; HFD, high-fat diet; HLP, hyperlipidemia; KEGG, Kyoto Encyclopedia of Genes and Genomes; LDL-C, low-density lipoprotein cholesterol; MF, Microctis Folium; PPAR-α, peroxisome proliferator-activated receptor; PPI, protein-protein interaction; SD, Sprague-Dawley; TG, triglycerides; TC, total cholesterol; TCM, traditional Chinese medicine; TCMSP, Traditional Chinese Medicine Systems Pharmacology.

Data Sharing Statement

Data will be made available on request.

Ethics Statement

All experimental protocols were designed according to the Guide for the Care and Use of Laboratory Animals (NIH Publication, 8th edition, 2011) and approved by the Ethics Committee of the Guangdong Provincial Engineering Technology Research Institute of TCM (approval number: 00416317).

Author Contributions

All authors made a significant contribution to the work reported, whether that is in the conception, study design, execution, acquisition of data, analysis and interpretation, or in all these areas; took part in drafting, revising or critically reviewing the article; gave final approval of the version to be published; have agreed on the journal to which the article has been submitted; and agree to be accountable for all aspects of the work.

Funding

The authors (s) declare that they have received financial support for the research, authorship, and/or publication of this article. This work was supported by the Basic and Applied Basic Research Foundation of Guangdong Province (Grant No. 2024A1515012809), Major Science and Technology Project on Traditional Chinese Medicine in Guangzhou (Grant No. 2025QN003), Scientific Research Project of Traditional Chinese Medicine Bureau of Guangdong Province (Grant No. 20251034), and University Hospital Joint Fund Project of Guangzhou University of Chinese Medicine (Grant No. GZYSE2024G07).

Disclosure

The authors declare no conflicts of interest.

References

1. Xiao G, Zeng Z, Jiang J, et al. Network pharmacology analysis and experimental validation to explore the mechanism of Bushao Tiaozhi capsule (BSTZC) on hyperlipidemia. *Sci Rep*. 2022;12(1):6992. doi:10.1038/s41598-022-11139-2
2. Dong P, Wang H, Li Y, et al. Active peptides from Eupolyphaga sinensis walker attenuates experimental hyperlipidemia by regulating the gut microbiota and biomarkers in rats with dyslipidemia. *Biomed Pharmacother*. 2024;170:116064. doi:10.1016/j.biopha.2023.116064
3. Zeng M, Qin X, Yi T, et al. Integration of pharmacodynamics, metabolomics and network pharmacology to elucidate the effect of Prunella vulgaris seed oil in the treatment of hyperlipidemia. *Arab J Chem*. 2024;17(2). doi:10.1016/j.arabjc.2023.105486
4. Meng H, Song J, Fan B, et al. Monascus vinegar alleviates high-fat-diet-induced inflammation in rats by regulating the NF-κB and PI3K/AKT/mTOR pathways. *Food Sci Hum Wellness*. 2022;11(4):943–953. doi:10.1016/j.fshw.2022.03.024
5. Bai Y, Jia Q, Su W, et al. Integration of molecular networking and fingerprint analysis for studying constituents in Microctis Folium. *PLoS One*. 2020;15(7):e0235533. doi:10.1371/journal.pone.0235533
6. Chen YG, Li P, Li P, et al. alpha-Glucosidase inhibitory effect and simultaneous quantification of three major flavonoid glycosides in Microctis folium. *Molecules*. 2013;18(4):4221–4232. doi:10.3390/molecules18044221
7. Xiao G, Jiang J, Li S, et al. Analysis of chemical constituents in Microctis Folium by UPLC-Q-TOF-MS/MS. *Chin J Exp Tradit Med Form*. 2021;27(3):138–148. doi:10.13422/j.cnki.syfjx.20201948
8. Huang Z, Song Y, Yan D. Investigation of ion liquid combined with ultrasound-assisted extraction technology of total flavones from Microcos paniculata and study on its lipids regulation activity. *Chin Tradit Herbal Drugs*. 2019;50(24):5995–6001. doi:10.7501/j.issn.0253-2670.2019.24.012
9. Su S, Xiang D, Liu X, et al. Effect and mechanism of Micrococtis Folinm on mouses with non-alcoholic fatty liver disease. *Chin J Exp Tradit Med Form*. 2018;24(1):130–135. doi:10.13422/j.cnki.syfjx.2018010130

10. Su S, Xiang D, Liu X. Impacts of Microcos Paniculata on blood lipid and antioxidant capacity in the rats of Hyperlipidemia. *World J Integr Tradit West Med*. 2016;11(11):1540–1543. doi:10.13935/j.cnki.sjzx.161117
11. Gong X, Li X, Xia Y, et al. Effects of phytochemicals from plant-based functional foods on hyperlipidemia and their underpinning mechanisms. *Trends Food Sci Technol*. 2020;103:304–320. doi:10.1016/j.tifs.2020.07.026
12. Taylor BA, Thompson PD. Statin-associated muscle disease: advances in diagnosis and management. *Neurotherapeutics*. 2018;15(4):1006–1017. doi:10.1007/s13311-018-0670-z
13. Feng L, Luo W. Mechanism analysis of paniculata total Alkaloids in Hyperlipidemia rats. *Med Innov China*. 2016;13(7):26–29. doi:10.3969/j.issn.1674-4985.2016.17.007
14. Lin S, Zeng X, Cai D. Analysis of the clinical efficacy of Paniculata with Tiaozhi decoction in the treatment of Hyperlipoidemia. *Mod Diagn Treat*. 2016;27(10):1790–1792.
15. Xiong H, Li N, Zhao L, et al. Integrated serum pharmacochemistry, metabolomics, and network pharmacology to reveal the material basis and mechanism of Danggui Shaoyao San in the treatment of primary Dysmenorrhea. *Front Pharmacol*. 2022;13:942955. doi:10.3389/fphar.2022.942955
16. Deng YY, Ma XY, He PF, et al. Integrated UPLC-ESI-MS/MS, network pharmacology, and transcriptomics to reveal the material basis and mechanism of Schisandra chinensis fruit mixture against diabetic nephropathy. *Front Immunol*. 2024;15:1526465. doi:10.3389/fimmu.2024.1526465
17. Zhang X, Zhang Q, Yu M, et al. Integrating serum pharmacochemistry and network pharmacology to explore the molecular mechanisms of Acanthopanax senticosus (Rupr. & Maxim.) Harms on attenuating doxorubicin-induced myocardial injury. *J Ethnopharmacol*. 2024;319(Pt 3):117349. doi:10.1016/j.jep.2023.117349
18. Wang L, Pu X, Nie X, et al. Integrated serum pharmacochemistry and network pharmacological analysis used to explore possible anti-rheumatoid arthritis mechanisms of the Shentong-Zhuyu decoction. *J Ethnopharmacol*. 2021;273:113988. doi:10.1016/j.jep.2021.113988
19. Bian X, Chen L, Bian X, et al. Protective effect of Tibetan medicine Qiwei Tiexie pills on liver injury induced by Acetaminophen overdose: an integrated strategy of network pharmacology, metabolomics and transcriptomics. *Phytomedicine*. 2024;123:155221. doi:10.1016/j.phymed.2023.155221
20. Yan P, Wei Y, Wang M, et al. Network pharmacology combined with metabolomics and lipidomics to reveal the hypolipidemic mechanism of Alismatis rhizoma in hyperlipidemic mice. *Food Funct*. 2022;13(8):4714–4733. doi:10.1039/d1fo04386b
21. Xiao G, Yang M, Zeng Z, et al. Investigation into the anti-inflammatory mechanism of Pothos chinensis (Raf.) Merr. By regulating TLR4/MyD88/NF-kappaB pathway: integrated network pharmacology, serum pharmacochemistry, and metabolomics. *J Ethnopharmacol*. 2024;334:118520. doi:10.1016/j.jep.2024.118520
22. Ge S, Liao C, Su D, et al. Wuwei Qingzhuo San Ameliorates Hyperlipidemia in mice fed with HFD by regulating metabolomics and intestinal flora composition. *Front Pharmacol*. 2022;13:842671. doi:10.3389/fphar.2022.842671
23. Du L, Wang Q, Ji S, et al. Metabolomic and Microbial Remodeling by Shanmei Capsule Improves Hyperlipidemia in High Fat Food-Induced Mice. *Front Cell Infect Microbiol*. 2022;12:729940. doi:10.3389/fcimb.2022.729940
24. Cai Z, He J, Jiang J, et al. Systematic investigation of the material basis, multiple mechanisms and quality control of Simiao Yong'an decoction combined with antibiotic in the treatment of sepsis. *Phytomedicine*. 2023;116:154910. doi:10.1016/j.phymed.2023.154910
25. Liu Y-M, Li X-Q, Zhang X-R, et al. Uncovering the key pharmacodynamic material basis and possible molecular mechanism of extract of Epimedium against liver cancer through a comprehensive investigation. *J Ethnopharmacol*. 2023;317:116765. doi:10.1016/j.jep.2023.116765
26. Xiu C, Luo H, Huang W, et al. Lobetyolin suppressed Osteoclastogenesis and alleviated bone loss in ovariectomy-induced osteoporosis via hindering p50/p65 nuclear translocation and downstream NFATc1/c-Fos expression. *Drug Design Develop Ther*. 2025;Volume 19:4689–4715. doi:10.2147/dddt.S515930
27. Lang J, Li L, Quan Y, et al. LC-MS-based metabolomics reveals the mechanism of anti-gouty arthritis effect of Wuwei Shexiang pill. *Front Pharmacol*. 2023;14:1213602. doi:10.3389/fphar.2023.1213602
28. Fan X, Zhang Y, Song Y, et al. Compound Danshen Dripping Pills moderate intestinal flora and the TLR4/MyD88/NF-κB signaling pathway in alleviating cognitive dysfunction in type 2 diabetic KK-Ay mice. *Phytomedicine*. 2023;111:15456. doi:10.1016/j.phymed.2023.154656
29. Lin J, Wang X, Gu M, et al. Geniposide ameliorates atherosclerosis by restoring lipophagy via suppressing PARP1/PI3K/AKT signaling pathway. *Phytomedicine*. 2024;129:155617. doi:10.1016/j.phymed.2024.155617
30. Zhang Y, Guo Z, Wang J, et al. Qinlian hongqu decoction ameliorates hyperlipidemia via the IRE1-alpha/IKKB-beta/NF-kappab signaling pathway: network pharmacology and experimental validation. *J Ethnopharmacol*. 2024;318(Pt A):116856. doi:10.1016/j.jep.2023.116856
31. Lv H, Yu Z, Zheng Y, et al. Isovitexin exerts anti-inflammatory and anti-oxidant activities on Lipopolysaccharide-induced acute lung injury by inhibiting MAPK and NF-kappaB and activating HO-1/Nrf2 pathways. *Int J Biol Sci*. 2016;12(1):72–86. doi:10.7150/ijbs.13188
32. Liu Y, Sun Z, Dong R, et al. Rutin ameliorated lipid metabolism dysfunction of diabetic NAFLD via AMPK/SREBP1 pathway. *Phytomedicine*. 2024;126:155437. doi:10.1016/j.phymed.2024.155437
33. Manzoni AG, Passos DF, Leitemperger JW, et al. Hyperlipidemia-induced lipotoxicity and immune activation in rats are prevented by curcumin and rutin. *Int Immunopharmacol*. 2020;81:106217. doi:10.1016/j.intimp.2020.106217
34. Li C, Chen Y, Yuan X, et al. Vitexin ameliorates chronic stress plub high fat diet-induced nonalcoholic fatty liver disease by inhibiting inflammation. *Eur J Pharmacol*. 2020;882:173264. doi:10.1016/j.ejphar.2020.173264
35. Zhu T, Huang X, Zhu H, et al. Analysis of bioactive components and synergistic action mechanism of ShuGan-QieZhi Capsule for treating non-alcoholic fatty liver disease. *Phytomedicine*. 2024;123:155173. doi:10.1016/j.phymed.2023.155173
36. Mokhtari I, Mokhtari C, Moumou M, et al. Polyphenol-rich extract from loquat fruit peel prevents hyperlipidemia and hepato-nephrotoxicity in mice: in vivo study and in silico prediction of possible mechanisms involving identified polyphenols and/or their circulating metabolites. *Food Funct*. 2023;14(16):7489–7505. doi:10.1039/d3fo01992f
37. Feng D, Zou J, Su D, et al. Curcumin prevents high-fat diet-induced hepatic steatosis in ApoE(-/-) mice by improving intestinal barrier function and reducing endotoxin and liver TLR4/NF-kappaB inflammation. *Nutr Metab*. 2019;16:79. doi:10.1186/s12986-019-0410-3
38. Chang H, Li X, Cai Q, et al. The PI3K/Akt/mTOR pathway is involved in CVB3-induced autophagy of HeLa cells. *Int J Mol Med*. 2017;40(1):182–192. doi:10.3892/ijmm.2017.3008

39. Han F, Xiao QQ, Peng S, et al. Atorvastatin ameliorates LPS-induced inflammatory response by autophagy via AKT/mTOR signaling pathway. *J Cell Biochem*. 2018;119(2):1604–1615. doi:10.1002/jcb.26320
40. Sun C, Zhang J, Hou J, et al. Induction of autophagy via the PI3K/Akt/mTOR signaling pathway by Pueraria flavonoids improves non-alcoholic fatty liver disease in obese mice. *Biomed Pharmacother*. 2023;157:114005. doi:10.1016/j.biopha.2022.114005
41. Cheng C, H LX, He J, et al. Apolipoprotein A4 restricts diet-induced Hepatic Steatosis via SREBF1-mediated lipogenesis and enhances IRS-PI3K-Akt signaling. *Mol Nutr Food Res*. 2022;66(18):e2101034. doi:10.1002/mnfr.202101034
42. Liu H, Li X, Duan Y, et al. Mechanism of gypenosides of Gynostemma pentaphyllum inducing apoptosis of renal cell carcinoma by PI3K/AKT/mTOR pathway. *J Ethnopharmacol*. 2021;271:113907. doi:10.1016/j.jep.2021.113907
43. Zhang J, Feng J, Bai Y, et al. Ameliorating the effect and mechanism of chitosan oligosaccharide on nonalcoholic fatty liver disease in mice. *Food Funct*. 2023;14(23):10459–10474. doi:10.1039/d3fo03745b
44. Bi S, Xu Z, Yuan A, et al. Elucidating the differential mechanisms of Jingui Shenqi Pill and Mingmu Dihuang Pill in the treatment of diabetic nephropathy based on Yin-Yang theory. *Drug Des Devel Ther*. 2025;19:2817–2831. doi:10.2147/DDDT.S517143
45. Li Y, Yin Y, Xiong J, et al. Combining Network Pharmacology and Transcriptomics to Investigate the Mechanisms of Yujiang Paidu Decoction in the Treatment of Chronic Rhinosinusitis with Nasal Polyps. *Drug Des Devel Ther*. 2024;18:3791–3809. doi:10.2147/DDDT.S461769